

Open-loop Verification of Motion Planning for an Underwater Eel-like Robot

Kenneth A. McIsaac and James P. Ostrowski
General Robotics Automation, Sensing and Perception Laboratory (GRASP)
University of Pennsylvania
Philadelphia PA 19104
{kamcisaa,jpo}@grip.cis.upenn.edu

Abstract: In this paper, we perform experimental verification of open-loop motion planning for a biomimetic robotic system using our underwater eel-like robot. Our results from past work provide theoretical justification for proposed gaits for forward/backward swimming, circular swimming, sideways swimming and turning in place. We have developed a five-link, underwater eel-like robot focusing on modularity, reliability and rapid prototyping, to verify our theoretical predictions. Results from experiments performed with this robot using visual position sensing in an aquatic environment show good agreement with theory.

1. Introduction and Background

Mobile robots continue to challenge researchers with new applications in a variety of environments. Of recent interest has been the application of robotic technology to underwater exploration, monitoring, and surveillance. In this paper, we explore the modeling, simulation, and design of controllers for snake-like robotic systems capable of both crawling overland and underwater swimming.

In recent research, *biomimetic* (biologically based) approaches to underwater locomotion have been pursued. The biomimetic approach to locomotion systems has several potential advantages, including increased underwater efficiency and agility. Recent research has explored various size ranges of robots, including the RoboTuna [15], and smaller fish-like projects [2, 5]. Less work has been done in the area of *anguilliform* (eel-like) locomotion, though recently Ekeberg [11] has simulated the motion of such systems when controlled by biologically based neural networks.

A central issue in studying mobile robots is how to enable a robot to move from one location to another, the *motion planning problem*. There is an extensive literature on motion planning [1, 7], though the vast majority has focused on kinematic systems in which the robot's motion can be described by a differential equation that is linear in the inputs, e.g., nonholonomic, car-like robots. More recently, however, researchers have begun to explore algorithms for developing the motion plans for robots with more complex governing equations, for example, in flexible part handling [4] or mobile manipulators with dynamics [12, 14, 16]

Our interest in this area has emerged from the study of underactuated dynamic mobile robots, ranging from the snakeboard [13] to a vision-guided blimp [17] to an *anguilliform* (eel-like) robot [8, 10], discussed in this paper.

In prior work, we have presented a proposed solution to the motion planning problem for the anguilliform robot. We use a geometric analysis of the dynamics of the robotic system to determine gaits for momentum generation [9], and a sampled feedback/feedforward approach to perform closed-loop steering control [10]. In this work, we verify our open-loop approach to momentum generation with our robotic eel using visual feedback to extract position information in an aquatic environment, and compare results from the robotic system to our simulated dynamic model. We present gaits for forward/backward and circular swimming, as well as novel gaits for sideways swimming and turning in place which were predicted in [9]. We also propose a simple extension to our open-loop system that will allow verification of our closed-loop steering control and accomplish full motion planning in the plane for the underwater, anguilliform robot.

2. Mathematical Model and Gait Selection

In [8], we studied anguilliform locomotion using a simplified physical model of a snake (we use the term “snake” interchangeably with “eel”) to be used as a platform to test various locomotive gaits (see also [11]). We model the snake as a planar, serial chain of identical links with mass m , length $2d$, and inertia J . We assume full control of the internal shape of the snake (the joint angles ϕ_i) which allows us to solve the dynamic equations in terms of the unknown configuration variables (x, y, θ) —the position and orientation of the middle link. The mechanical robot used in this work is a five link model. It is advantageous to choose an odd number of links to gain symmetry about the central link. Figure 1(A) shows the three link case.

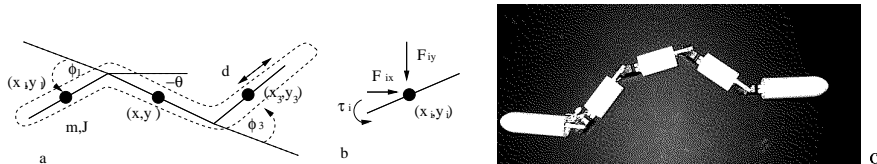


Figure 1. (a) Model of snake, (b) Forces and torques on link i , (c) The REEL II eel robot.

2.1. Friction Models

The crucial elements in this model are the drag force terms, which generate the locomotion. To simulate the forces in the water, we adopt a simple fluid mechanical model. We assume that the Reynolds number is high enough that inertial forces dominate over viscous effects—a reasonable approximation for smooth bodies in water. We also assume that the fluid is stationary, so the force of the fluid on a given link is due only to the motion of that link. The pressure differential created by an object moving in a fluid causes a drag force opposing the motion. Under the assumptions above, the drag force developed takes the form $F \propto \mu_w v^2$. Here, v is the forward speed of the link and μ_w is a drag coefficient for the water, determined by the formula $\mu_w = \rho AC/2$, where A is the effective area of the object, ρ is the density of water, and C is a shape coefficient.

In our simulations, we assume that pressure differentials in the directions

parallel to the moving body are decoupled from pressure differentials perpendicular to the body, to yield:

$$F_i^\perp = -\mu_w \text{sgn}(v_i^\perp) \cdot (v_i^\perp)^2 \quad (1)$$

where v_i^\perp is the projection of the vector (\dot{x}_i, \dot{y}_i) along a direction perpendicular to the link. We exclude drag forces parallel to the link because they were determined in simulation to have negligible effects. The discontinuity in $\text{sgn}(v)$ means that this expression is not tractable for use in calculations. Therefore, in our analytical derivations we use an approximation to this function, which turns out to be linear in v :

$$F_{\text{approx}} = \mu v^\perp \quad (2)$$

where μ is defined by a least squares fit over a small range around $v = 0$. We also note that this force model can be interpreted as a viscous damping model, as might be encountered with a snake moving over soft sand.

2.2. Equations of Motion

The derivation of the system of equations governing the time evolution of the system momentum is involved, and presented in detail elsewhere [8]. We present a brief synopsis here.

The system state is governed by the time-evolution of the (body-referenced) velocity vector ξ , which describes forward, sideways and turning velocities, and by the time-evolution of the generalized momentum vector p of momentum in the three body-referenced dimensions. Starting from the Lagrangian formulation of the equations of motion and taking advantage of the invariance of the system with respect to changes in position and orientation, we are able to express the equations of motion by:

$$\dot{\xi} = -\mathbb{A}(r)\dot{r} + I^{-1}(r)p, \quad (3)$$

$$\dot{p} = \dot{r}^T \sigma_{\dot{r}\dot{r}}(r)\dot{r} + p^T \sigma_{p\dot{r}}(r)\dot{r} + p^T \sigma_{pp}(r)p + \tau_g \quad (4)$$

where \mathbb{A} , I , $\sigma_{\dot{r}\dot{r}}$, $\sigma_{p\dot{r}}$ and σ_{pp} depend on the system geometry. Using the force approximation given in Equation 2, the external forces τ can be expressed:

$$\tau_i = \alpha(r)_i^j p_j + \eta(r)_{ij} \dot{r}^j \quad (5)$$

2.3. Perturbation Analysis

In order to gain some insight into the effect of gait selection on the time evolution of the momentum, we use a perturbation approach, making the assumption that the joint angles vary sinusoidally around some initial value. We set $r^j(t) = r_0^j + \epsilon r_1^j(t)$ (introducing a scaling parameter ϵ) in Equation 5, and solve for the momentum in ascending orders of ϵ ($p_i = p_{i0} + \epsilon p_{i1} + \epsilon^2 p_{i2} + \dots$) using Equation 4. With the assumption that $p(0) = 0$, we see immediately that $p_{i0} = 0$ for all time. We can also show that p_{i1} will have zero average using cyclic inputs. We conclude that, to second order in ϵ the momentum is dominated by:

$$\dot{p}_{i2} = \alpha(r_0)_i^j p_{j2} + r_1^j \kappa(r_0)_{ijk} \dot{r}_1^k \quad (6)$$

where the tensor $\kappa_{ijk} = \frac{\partial \eta_{ik}}{\partial r_j}$ has been introduced. (Other terms appear in this equation—for example, a term of the form $\frac{\partial \alpha}{\partial r} p_1 r_1$, but their affect was determined to be negligible using numerical solution of the equation, so they have been ignored.) This is a simple, first-order dynamic equation, parametrized by the gait parameter r_0 . Using this equation, we are able to propose gait selection criteria for the eel.

2.4. Gait Selection Criteria

Equation 6 allows us to select appropriate gait waveforms to accomplish arbitrary maneuvers in the water. The α and κ tensors, affected by the choice of r^i , determines the coupling between momenta in the three planar dimensions. By careful choice of gait inputs, we can decouple forward motion, sideways motion and rotary motion, or couple them to accomplish, for example, circular trajectories.

We limit our attention to travelling wave gaits of the form:

$$r^i(t) = \epsilon \sin(\omega t + A(i)\phi_s) + B(i)\phi_{\text{offs}} \quad (7)$$

for some amplitude ϵ , frequency ω , phase-shift ϕ_s and turning offset ϕ_{offs} (the functions $A(i)$ and $B(i)$ are link-dependent parameters controlling phasing and steering offset). Even using this simple, restricted gait model, we are able to accomplish the following modes of locomotion:

- Forward motion, using $A(i) = -i$ and $\phi_{\text{offs}} = 0$ as above.
- Backward motion, using $A(i) = i$ and $\phi_{\text{offs}} = 0$.
- Circular motion, forwards or backwards, using $\phi_{\text{offs}} \neq 0$. The sign of ϕ_{offs} will determine the direction of the turn, and the turning radius will be inversely related to its magnitude.
- Sideways motion, using $A > 0$ for $i < N/2$, $A < 0$ for $i > N/2$, $B > 0$ for $i < N/2$ and $B > 0$ for $i > N/2$. (Pairs of signs may be reversed, to change direction).
- Turning in place, using $A > 0$ for $i < N/2$, $A < 0$ for $i > N/2$, $B > 0$ for $i < N/2$ and $B < 0$ for $i > N/2$. (Pairs of signs may be reversed, to change direction).

3. Robot Design and Experimental Setup

In [8] we presented the design of the REEL (Robotic EEL), a radio controlled robot used to perform preliminary, qualitative verification of our control algorithm. The REEL consisted of four identical links, and used a rubber tube as its waterproof “skin”. In this work, we developed a second generation version of this robot (the REEL II—see Figure 1), which addressed some difficulties in the first design and has performed admirably in experimental testing. The rubber “skin” used in the original design was determined to be inappropriate, since replacement of a malfunctioning part (or discharged battery) required removal of the entire skin—a difficult procedure. The use of external skin as a waterproofing agent is also a poor choice. The skin must have a re-sealable opening (to allow access for maintenance), which becomes a point of failure since re-sealing

is often done haphazardly, especially during field trials. Finally, it is difficult to find waterproof materials which are flexible enough to permit shape changes without resistance, but rigid enough to hold a hydrodynamic cross-section.

The solution adopted in REEL II (see Figure 1) was to design plastic links in the shape of elliptical cylinders (rounded nose cones were attached to the head and tail links to achieve a streamlined hydrodynamic profile). We manufactured these links using a fused deposition modeling (FDM) machine. The electronic parts (servo-motors, radio receiver and battery) were individually, permanently waterproofed using an epoxy resin sealant. A waterproof connector capable of “wet” insertion was used for the power supply connection, to enable easy battery replacement in the field. Because our links are made of interchangeable, identical parts, we have a robust, modular design for the robot. During testing, the robot was dropped, breaking one of the servo-motors. The motor was replaced without any modifications being needed to the rest of the robot.

The robot shape is radio-controlled. A PC ground station calculates the shape variables (joint angles), which are transmitted using an off-the-shelf radio controller to a receiver in the nose of the robot. The joint actuators are position controlled, medium-torque servo-motors with a specified maximum angular velocity of $315^\circ/sec$, and an maximum angular velocity in water (observed) of $45^\circ/sec$, which enables 0.5 Hz operation for the robot. The robot operates for approximately 20 minutes using a 600mAh battery.

4. Experimental Results and Analysis

4.1. Visual position sensing

We perform our open-loop experiments using a fixed, digital camera to record the behaviour of the robot in a pool of still water. Image processing is performed off-line, in real-time using the Matrox Imaging Library software. We use edge detection, followed by a closing operation to locate the robot as a single blob in the image. The robot’s position and orientation in the image plane are determined from the centroid and orientation of this blob. Figure 2(a) shows a sample frame of captured video, and Figure 2(b) shows the post-processed image used in feature extraction.

Once data is available in the image plane, we are able to extract real-world coordinates by unwarping the data. We use the position of fixed reference points in the image to determine the appropriate transformation to yield the robot’s true position and orientation in the pool.

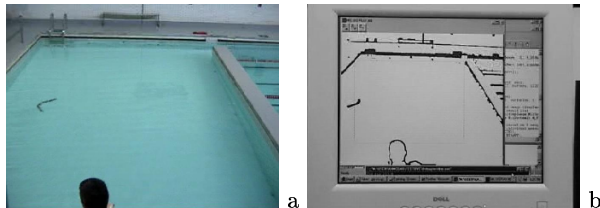


Figure 2. Experimental images (a) Raw image. (b) Post-processed image.

Our mathematical model of the eel in water leads to two non-dimensional parameters that influence the dynamics in water: an inertia parameter, $\hat{J} =$

J/md^2 , and a drag parameter $\hat{\mu} = \mu/m$. Using data from one experiment, we tuned the drag parameter until our simulations matched observed data for all experiments, except for one case (sideways swimming) which we will describe below. We can conclude that our friction model has sufficient predictive power to be used for the development of open loop controls. We also demonstrate the necessity for feedback, since the match between observed and predicted open-loop paths is only approximate.

4.2. Forward motion

The first gait we explored is a simple travelling wave gait used for forward motion. This gait is a discrete approximation to the *serpenoid curve*, which Hirose [3] proposed as the true gait used by crawling snakes, and has also been justified by our perturbation analysis of the dynamics of the eel [9]. We use:

$$\phi_i(t) = A \sin(\omega t + i\phi_s) \quad (8)$$

for amplitude $A = \pi/6$, frequency $\omega = \pi$ and phase shift $\phi_s = \pi/3$. Our choices of amplitude and frequency were motivated by physical limits in the robot, while the choice of phase ϕ_s was motivated by our perturbation analysis [9] which predicted that 60° is the optimal gait phase for a five link snake. To compare observed data to predictions, we used our full dynamic model with the quadratic fluid drag approximation introduced in Section 2.1 and tuned the fluid drag parameter μ_w . The best match to observed data was found when $\mu_w = 0.15$, which differs from the theoretical value taken from Ekeberg [11] ($\mu_w = 0.45$) but is of the same order of magnitude. Figure 3(a) is a plot of observed vs. simulated data for 20 seconds using these parameter values. The path followed by the robot in the water (solid curve) does not display the oscillations of the simulated data because the vision algorithm samples a center of mass position, whereas the simulated data is the position of the center of one link. We also note that the observed path deviates from a straight line. This justifies our expectation that feedback will be needed to perform true motion planning for the eel robot—open loop operation is not sufficient to follow planned trajectories.

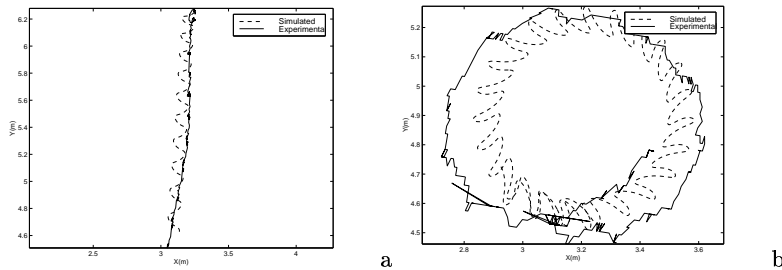


Figure 3. Simulated and experimental data for the (a) forward and (b) circular drive gaits. Simulated data is shown dashed, and experimental data solid.

4.3. Circular paths

We next explored our proposed gait for circular motion. The circular gait is another travelling wave gait, with a steering offset introduced to create a bias in

the momentum generated during each cycle. We had qualitative justification of this gait in our experiments with the original REEL I robot, as well as theoretical justification in our perturbation analysis of the dynamics of the eel [9]. The joint angles ϕ_i take the form:

$$\phi_i(t) = A \sin(\omega t + i\phi_s) + \phi_{\text{offs}} \quad (9)$$

for amplitude $A = \pi/6$, frequency $\omega = \pi$ and phase shift $\phi_s = \pi/3$ and offset $\phi_{\text{offs}} = \pi/12$. Our choices of amplitude, frequency and offset were motivated by physical limits in the robot, while the choice of phase ϕ_s was motivated by our perturbation analysis as in Section 4.2. We compared observed data to predicted data using our full dynamic model with the quadratic fluid drag approximation and the μ_w parameter as tuned in our forward gait experiment. Figure 3(b) is a plot of observed versus simulated data for approximately 40 seconds using these parameter values. As in the case of forward swimming, the actual path deviates from a perfect circle, however the robot follows a closed elliptical path with only minor eccentricity, validating our choice of circular turning gait.

4.4. Turning in place

The third gait tested was a novel gait, predicted by our perturbation analysis (see Section 2.3) for turning in place. This gait essentially consists of two reinforcing travelling waves propagating outwards from the central link.

In this case, we use joint angles of the following form:

$$\phi_i = \begin{cases} A \sin(\omega t - (N/2 - i)\phi_s) - \phi_{\text{offs}} & 1 \leq i \leq N/2 \\ A \sin(\omega t - (i - 1 - N/2)\phi_s) + \phi_{\text{offs}} & N/2 < i \leq N \end{cases}$$

for $N = 4$, the number of joints, for amplitude $A = \pi/6$, frequency $\omega = \pi$ and phase shift $\phi_s = \pi/2$ and offset $\phi_{\text{offs}} = \pi/12$. Our choices of amplitude, frequency and offset were motivated by physical limits in the robot, while the choice of phase ϕ_s was motivated by our perturbation analysis [9] which predicted that 90° is the optimal gait phase for a three-link snake. (The turn-in-place gait can be viewed as two three-link snakes connected at the tail, each attempting to turn in the same direction.) We compared observed data to predicted data using our full dynamic model with the quadratic fluid drag approximation and the μ_w parameter as tuned in our forward gait experiment (see Section 4.2). Figure 4(a) is a plot of observed versus simulated orientation for 20 seconds using these parameter values. Figure 4(b) plots observed robot position versus time for the same 20 seconds, to show that the robot is not moving.

4.5. Sideways swimming

The final gait tested in our experiments was another novel gait, predicted by our perturbation analysis [9] for sideways swimming. This gait essentially consists of two opposing travelling waves propagating outwards from the central link, and is reminiscent of the backstroke used by human swimmers.

In this case, we use joint angles of the following form:

$$\phi_i = \begin{cases} A \sin(\omega t - (N/2 - i)\phi_s) + \phi_{\text{offs}} & 1 \leq i \leq N/2 \\ A \sin(\omega t - (i - 1 - N/2)\phi_s) + \phi_{\text{offs}} & N/2 < i \leq N \end{cases}$$

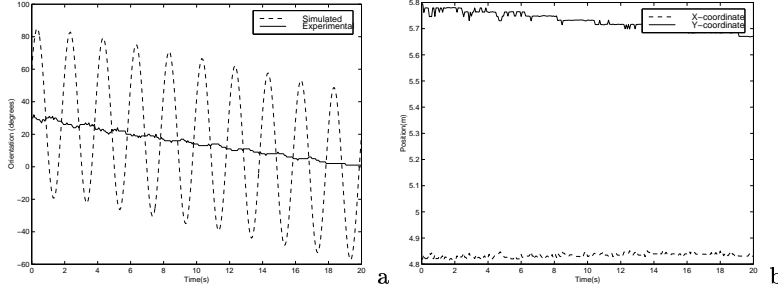


Figure 4. (a) Simulated and experimental data for the turn in place drive gait. Simulated data is shown dashed, and experimental data solid. (b) Position data for the turn in place gait. Note that the robot only drifts a total of 10cm.

for $N = 4$, the number of joints, for amplitude $A = \pi/6$, frequency $\omega = \pi$, phase shift $\phi_s = \pi/2$ and offset $\phi_{\text{offs}} = \pi/12$. Our choices of amplitude, frequency and offset were motivated by physical limits in the robot, while the choice of phase ϕ_s was motivated by our perturbation analysis which predicted that 90° is the optimal gait phase for a three-link snake. (The sideways gait can be viewed as two three-link snakes connected at the tail, attempting to turn in opposing directions.) We compared observed data to predicted data using our full dynamic model with the quadratic fluid drag approximation and the μ_w parameter as tuned in our forward gait experiment (see Section 4.2). As is evident in Figure 5, there is considerable discrepancy in the observed and predicted behaviour of the robot using this gait. In fact, even attempting to tune the fluid drag coefficient parameter μ_w , we were unable to match our observed data. We provide a possible explanation below in Section 5.

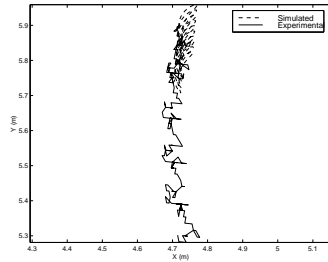


Figure 5. Simulated and experimental data for the sideways gait. Simulated data is shown dashed, and experimental data solid. Notice that there is a large discrepancy between predicted and actual performance.

5. Discussion of Experimental Results

In general, our experimental data show good agreement with predictions. Gaits for forward motion, motion in circular paths and turning in place have been verified experimentally, and we see that we are able to tune our simulations to match experimental data simply with modifications to one fluid drag parameter.

Our closed loop control algorithm presented in [10] used a feedforward approach to improve turning performance by precalculating necessary steering offsets. Since we are able to tune our simulation to match experimental results, it should be possible to determine these open-loop steering commands in simulation with a reasonable expectation of success in closed-loop control.

We have also verified our choice of vision-based position sensing for closed-loop control. Open-loop motion planning will not suffice in our real-world setting since there are deviations from predicted paths. Visual feedback provides a cheap position sensor that does not need to be waterproofed. We are able to capture data in real-time (15 frames/second), which meets our closed-loop requirements, since our control algorithm [10] is based on averaged sampling over one gait cycle (0.5Hz).

We observed minor errors in our experimental trajectory. The most likely sources of these discrepancies is that our simulations are based on an idealized model of the discrete eel that does not perfectly reflect some of the features of the robot. We have assumed that the robot is symmetric for modelling and simulation. In fact, it is not symmetric—the first and last links are approximately 50% longer than middle links, and the first link is both heavier than other links (due to the presence of the battery), and has increased drag, due to the presence of the battery cable which drags outside the link. It is also possible that small currents exist in the pool due to filtration. Open-loop control will not correct for such disturbances. Finally, we believe there are infrequent errors in the radio-communication protocol that lead to “glitches” or “spasms” in the gait waveform as motors receive discontinuous angular commands. These have the effect of causing one-time disturbances or “kinks” in the trajectory.

The only major discrepancy between predicted and observed data comes in the case of the sideways gait. The gait performed considerably *better* than expected—robot velocities were almost an order of magnitude higher than predictions! We are able to propose one possible explanation for this. Our model and simulations are based on a simple fluid dynamic approach that considers *only* drag forces on the links and completely neglects the phenomenon of momentum shedding and thrust in the wake. Under conditions of a slender body undergoing small oscillations, this is a reasonable approximation, however in the case of our proposed sideways gait, these conditions are not met, since the robot has a very large cross section in the direction of motion and is undergoing large shape changes. The excess momentum generated is likely caused by some sort of thrust or wake effect that would have to be modelled by some form of carangiform (fish-like) swimming [5, 6].

6. Conclusions and Future Work

We have developed an experimental system to evaluate the open-loop performance of a biomimetic, underwater eel-like robot. Using predictions from theory made in prior work on the analysis of the system dynamics [9], we tested five drive gaits for various modes of locomotion. Our robot performed well in these tests, despite some experimental errors due to asymmetry in the robot implementation. We have a robust, modular robotic design that will be a useful platform for future experiments.

In future work, we plan to extend our experimental analysis of the system. In prior work [10], we proposed an algorithm for closed-loop control of the

eel, using visual feedback. We can implement this control scheme in our test platform with only software modifications. We also plan to add new degrees of freedom to the robot to enable motion in the vertical dimension, so we will not be restricted to the plane.

References

- [1] R. W. Brockett and L. Dai. Nonholonomic kinematics and the role of elliptic functions in constructive controllability. In Z. Li and J. F. Canny, editors, *Nonholonomic Motion Planning*, pages 1–21. Kluwer, 1993.
- [2] K. Harper, M. Berkemeier, and S. Grace. Decreasing energy costs of swimming robots through passive elastic elements. In *Proc. IEEE Int. Conf. Robotics and Automation*, pages 1839–1844, Albuquerque, NM, April 1997.
- [3] S. Hirose. *Biologically Inspired Robots: Snake-like Locomotors and Manipulators*. Oxford University Press, Oxford, 1993. Translated by Peter Cave and Charles Goulden.
- [4] L. Kavraki and F. Lamiroux. A general framework for planning paths for elastic objects. Submitted to the *International Journal of Robotics Research*, 1999.
- [5] S. D. Kelly, R. J. Mason, C. T. Anhalt, R. M. Murray, and J. W. Burdick. Modelling and experimental investigation of carangiform locomotion for control. In *Proc. of the American Control Conference (ACC)*, 1998. (submitted).
- [6] S. D. Kelly and R. M. Murray. Lagrangian mechanics and carangiform locomotion. In *Nonlinear Control Systems Design (NOLCOS)*, Enschede, The Netherlands, July 1998.
- [7] J.-C. Latombe. *Robot Motion Planning*. Kluwer, Boston, 1991.
- [8] K. A. McIsaac and J. P. Ostrowski. A geometric approach to anguilliform locomotion: Simulation and experiments with an underwater eel robot. In *Proc. IEEE Int. Conf. Robotics and Automation*, volume 1, pages 2843–2848, Detroit, MI, 1999.
- [9] K. A. McIsaac and J. P. Ostrowski. A geometric approach to gait generation for the anguilliform robot. In *Proc. of Int. Conf. on Intelligent Robots and Systems (IROS 2000)*, volume 1, pages 2230–2235, Tokyo, October 2000.
- [10] K. A. McIsaac and J. P. Ostrowski. Motion planning for dynamic eel-like robots. In *Proc. IEEE Int. Conf. Robotics and Automation*, volume 1, pages 1695–1700, San Francisco, CA, 2000.
- [11] Örjan Ekeberg. A combined neuronal and mechanical model of fish swimming. *Biological Cybernetics*, 69:363–374, 1993.
- [12] J. P. Ostrowski. Steering for a class of dynamic nonholonomic systems. *IEEE Transactions on Automatic Control*, 45(8):1492–1498, August 2000.
- [13] J. P. Ostrowski and J. W. Burdick. The geometric mechanics of undulatory robotic locomotion. *International Journal of Robotics Research*, 17(7):683–702, July 1998.
- [14] J. P. Ostrowski, J. P. Desai, and V. Kumar. Optimal gait selection for nonholonomic locomotion systems. *International Journal of Robotics Research*, 19(3):225–237, March 2000.
- [15] M. S. Triantafyllou and G. S. Triantafyllou. An efficient swimming machine. *Scientific American*, pages 64–70, March 1995.
- [16] M. Zefran, J. P. Desai, and V. Kumar. Continuous motion plans for robotic systems with changing dynamic behavior. In *Workshop on Algorithmic Foundations of Robotics (WAFR) '96*, Toulouse, France, July 1996.
- [17] H. Zhang and J. P. Ostrowski. Visual servoing with dynamics: Control of an unmanned blimp. In *Proc. Int. Conf. on Robotics and Automation*, pages 618–623, Detroit, MI, May 1999.